

ASME Journal of Engineering for Gas Turbines and Power Online journal at:

https://asmedigitalcollection.asme.org/gasturbinespower



Alexandre Guille¹

Institute of Fluid Dynamics, Helmholtz-Zentrum Dresden-Rossendorf, Dresden 01328, Germany e-mail: a.guille-bourdas@hzdr.de

Malini Bangalore Mohankumar

Institute of Fluid Dynamics, Helmholtz-Zentrum Dresden-Rossendorf, Dresden 01328, Germany

Sebastian Unger

Institute of Fluid Dynamics, Helmholtz-Zentrum Dresden-Rossendorf, Dresden 01328, Germany

Uwe Hampel

Institute of Fluid Dynamics,
Helmholtz-Zentrum Dresden-Rossendorf,
Dresden 01328, Germany;
Chair of Imaging Techniques in Energy and
Process Engineering,
Institute of Power Engineering,
Technische Universität Dresden,
Dresden 01328, Germany

Numerical Modeling of a Primary Heat Exchanger in sCO₂ Power Cycles for Thermal Energy Storage Systems

Renewable energy sources are the key for long-term decarbonization of energy. However, the intermittent nature of renewables does not always meet the energy demand in the electrical grid. Thus, electrical heated thermal energy storage systems (TES) coupled with sCO₂ power cycles are investigated at Helmholtz-Zentrum Dresden-Rossendorf as a possible solution to balance this mismatch. In this study, a printed circuit heat exchanger (PCHE) is considered as candidate for the 1 MW primary heat exchanger, given the mechanical challenge induced by drastic pressure difference between the hot fluid of the TES and the cold fluid of the power cycle. The present work consists of two parts, one elaborates a one-dimensional (1D) model in order to optimize the PCHE regarding the pump power required to compensate the pressure loss. It was found that the hot fluid coming from the TES accounts for 80% of the total pump power after optimization because of its low density and its high mass flow rate. Furthermore, three-dimensional simulations by computational fluid dynamics (CFD) were done and compared to the results from the 1D model to ensure its validity. It was observed that the results from the 1D model and the CFD simulations are consistent, with a slight potential deviation in the calculation of the pressure profile. [DOI: 10.1115/1.4066892]

Keywords: heat exchanger, printed circuit heat exchanger, supercritical CO_2 , ID model, computational fluid dynamics, Brayton power cycle, thermal energy storage

1 Introduction

Energy storage systems are key to increase the reliability of renewable energy sources. Within this framework, Thermal Energy Storage systems (TES) coupled with a power cycle have gained popularity since they can store energy from renewable sources during the periods of high production and release it when necessary. Figure 1 depicts an example of such a coupled system.

During the charging cycle, an electrically heated fluid flows into a solid thermal energy storage, whose temperature can reach up to $800\,^{\circ}\mathrm{C}$ [1], while the pressure is low, under 5 bar, to prevent mechanical problems [2]. During the discharging cycle, the same fluid enters the TES at temperatures lower than the TES. The fluid temperature is increased by the hot solid material before entering a heat exchanger, referred to as the Primary Heat Exchanger (PHX), to transfer the thermal energy to an sCO₂ power cycle.

Regarding the power cycle, since the temperature of the fluid entering the PHX is relatively high, Dostal et al. [3] showed that sCO₂ Brayton cycles present a higher efficiency than a traditional water Rankine cycle, when the turbine inlet temperature reaches 550 °C or higher. In fact, beyond the critical point, the viscosity of CO₂ drops while the density is high due to the high pressure. This

Turbo Expo, June 24-28, 2024. GT2024.

¹Corresponding author.

results in low compression work and thus increases the overall cycle efficiency [4]. Moreover, sCO₂ is nontoxic, inert and its cost is only 1/10 of helium and 1/70 of the organic fluid R134a [5]. Besides the numerous advantages of sCO₂ Brayton cycle, CO₂ hits the supercritical state at moderate pressure and temperature of 73 bar and 31.3 °C. Even though the pressure of sCO₂ in the PHX may change accordingly to the specific application, it can reach 200 bar in case of electricity generation [6,7]. Thus, the difference of pressure and the fluid properties in the PHX between the hot fluid, of the TES, and the cold fluid, of the power cycle, are unusually high. For this study, CO₂ at atmospheric pressure and supercritical CO₂ are chosen as working fluids, resulting in a challenging design regarding mechanical fluid-dynamic consideration.

One of the most promising candidates as PHX is the Printed Circuit Heat Exchanger (PCHE). For this heat exchanger grooves are etched on the top of multiple plates, the plates are stacked on top of each other and finally the etched plates are bounded by diffusion bonding. Thus, the grooves become the flow channels for the hot and the cold fluid. The channel patterns can be different and researchers studied several channel designs to improve the heat transfer performance (Fig. 2). Most of sCO₂ Brayton cycles in literature are heated by an electrical heater [5] or by waste heat [8], while they use PCHEs as recuperators. PCHEs reach high compactness and high efficiency with a typical channel diameter of 1 mm. Nonetheless, both fluids in the recuperators are supercritical, resulting in moderate pressure difference, which is not the case for a TES/sCO₂

Manuscript received September 23, 2024; final manuscript received October 10, 2024; published online December 20, 2024. Editor: Jerzy T. Sawicki.

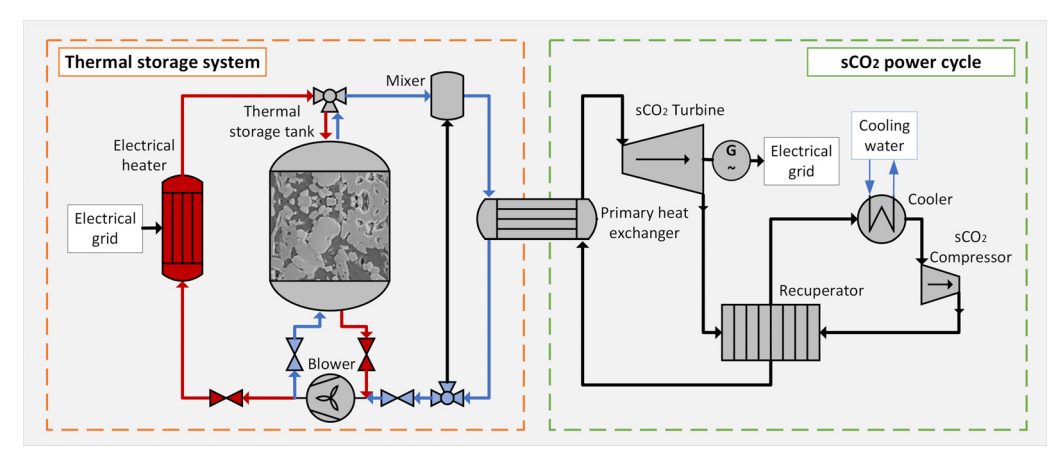


Fig. 1 Schematic of TES system coupled with an SCO₂ power cycle

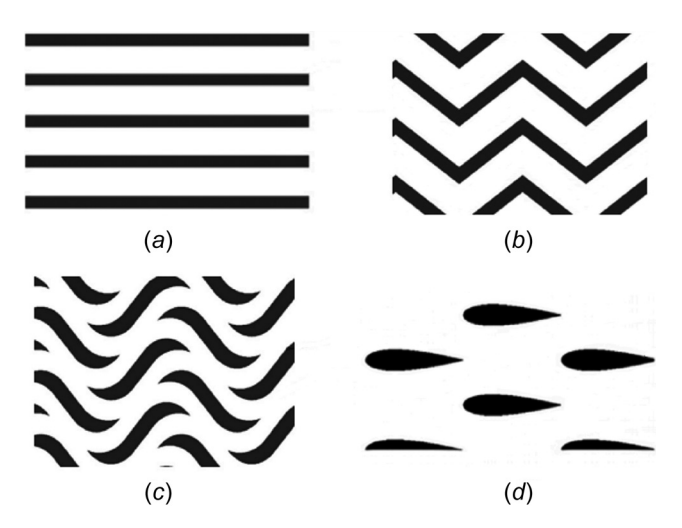


Fig. 2 Most studied designs for PCHE channel. (a) straight channels, (b) zigzag channels, (c) S-shaped fins, and (d) airfoil fins [10].

Brayton cycle application. However, since the development of Concentrated Solar Power (CSP) plants, the storage system and the power cycle are jointly studied. Actually, molten salt at atmospheric pressure is commonly used as hot fluid in the storage system to transport the heat, despite corrosion issue at high temperature [9].

Shi et al. [11] studied the heat transfer mechanisms and friction losses of a molten-salt/sCO₂ PCHE with airfoil fins for the hot plate and straight channels for the cold plate by means of computational fluid dynamics (CFD). They showed that the three-dimensional numerical model solved with the Re-Normalisation Group k- ε is accurate to their previous experiments with a maximum deviation of 12%. However, such an approach by methods like CFD has high computational costs, especially during the mesh validation. Zhu et al. [12] used the Logarithmic Mean Temperature Difference (LMTD) method to design and evaluate the costs of a 2 MW PCHE. The LMTD method is valid and precise, when thermal properties are constant, which is not always the case for supercritical fluids or when the temperature of the fluid changes drastically. Marchionni et al. [13] elaborated a one-dimensional (1D) model that discretizes the channels along the flow direction and the nodal model was validated by available data from literature. Yet, they studied the PCHE as a recuperator and not as a PHX. Therefore, the diameters for hot and cold fluids are equally designed, as the fluids have the same viscosity. Jiewei et al. [14] suggested to increase the diameter of the hot channels only, when molten salt is used, since its viscosity is much lower than for sCO_2 .

Most articles were investigating the heat transfer behavior and heat exchanger design of PCHE as a recuperator in sCO₂ power cycles or the heat transfer for molten salt as a fluid for thermal energy storages. However, the heat transfer from a solid thermal energy storage by a low-pressure gas, such as ambient-pressure CO_2 , to a high-pressure sCO_2 fluid stream, has received little attention yet. Thus, the purpose of the present paper is to elaborate a 1D model of the straight and zigzag channel design with CO_2 at atmospheric pressure as hot fluid and high pressure sCO_2 as cold fluid. Based on this model, a cost analysis is conducted to determine the optimized geometric parameters accordingly to a given set of boundary conditions. Finally, CFD simulations are conducted to ensure the model validity and investigate more detailed thermo-fluid-dynamic phenomena.

2 Materials and Methods

2.1 Thermal Resistance Network-Based Model and Optimization. A thermal resistance network (TRN) based 1D model is developed for modeling the heat transfer and pressure drop mechanisms that occur in the channels of the PCHE. Its first purpose is to determine the temperature and pressure profiles for a given set of thermal boundary conditions.

The model relies on the following assumptions: (1) the entrance effects are neglected and the flow is uniformly distributed. Thus, an elementary heat transfer unit is defined as a periodical element of the heat exchanger as shown on Fig. 3. (2) Regarding the fluid properties, they are supposed to be temperature and pressure dependent. However, it is assumed that the pressure drop does not have an impact on the variation of the fluid properties. To that extent, the temperature profile is first calculated independently from the pressure profile.

The total height H_{total} , width W_{total} and length L_{total} are set to match the maximum values found in the literature: $1 \text{ m} \times 1.5 \text{ m} \times 0.6$ [15]. In addition, the channels are discretized into $N_{\Delta x}-1$ elements with respect to general flow direction as well (Fig. 4). Thus, there are $N_{\Delta x}$ values for each fluid temperature profile and $N_{\Delta x}-1$ values for the wall temperatures, bringing the number

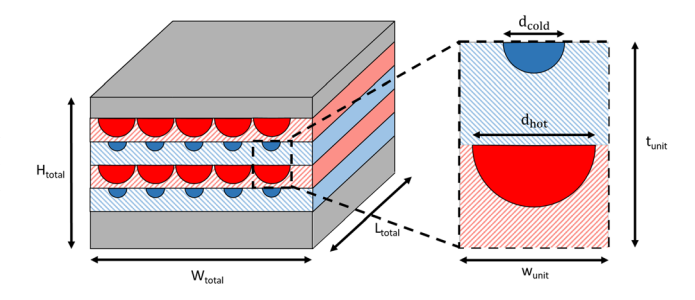


Fig. 3 Cross-view section of the PCHE and its elementary heat transfer unit

Table 1 Nusselt number correlations in a straight channel [16]

Correlation	Expression
Hesselgreaves	$\begin{aligned} \text{Nu} &= 4.089 \\ \text{Re} &\leq 2300 \end{aligned}$
Abraham	$Nu = 3.5239 \left(\frac{Re}{1000}\right)^4 - 45.148 \left(\frac{Re}{1000}\right)^3 + 212.13 \left(\frac{Re}{1000}\right)^2 - 427.45 \left(\frac{Re}{1000}\right) + 316.08$ $2300 \le Re \le 3100$
Gnielinski	$\begin{aligned} \text{Nu} &= \frac{\frac{f}{2}(\text{Re} - 1000)\text{Pr}}{1 + 12.7\sqrt{\frac{f}{2}}(\text{Pr}^{2/3} - 1)} \\ &3100 \leq \text{Re} \leq 5 \cdot 10^6 \\ &0.5 \leq \text{Pr} \leq 2000 \end{aligned}$

Table 2 Nusselt number correlations in a zigzag channel [17]

Correlation	Expression
Yoon (1)	$Nu = 5.05 + (0.02 \cdot \alpha + 0.003)RePr^{0.6}$
	$Re \le 450$
	$5 \deg \le \alpha \le 15 \deg$
Yoon (2)	Nu = $(0.18 \cdot \alpha + 0.457) \left(\frac{l_r}{d_h}\right)^{-0.038}$
	$Re^{\left(-0.23(\alpha-0.74)^2-0.004\left(\frac{l_r}{d_h}\right)\alpha+0.56\right)}$ Pr ^{0.58}
	450 ≤ Re
	$5 \deg \leq \alpha \leq 45 \deg$
	$4.09 \leq \frac{l_r}{d_h} \leq 32.73$

of nodal temperatures to $4N_{\Delta x}-2$. Then, the flux between each temperature is assimilated into a network of thermal resistances. The convective heat transfer is modeled by Newton's law as

$$Q_{\Delta x} = h \cdot A_{\Delta x} \cdot \Delta T \tag{1}$$

where $Q_{\Delta x}$ is the heat exchanged through the exchange surface area $A_{\Delta x}$ of a small element, ΔT is the temperature difference between the fluid and the wall, and h is the convective heat transfer coefficient. Its expression is based on the correlation of the Nusselt Nu number defined as

$$Nu = \frac{h \cdot d_h}{\lambda_f},\tag{2}$$

where λ_f is the thermal conductivity of the fluid and d_h is the hydraulic diameter, whose expression is

$$d_h = d\frac{\pi}{\pi + 2},\tag{3}$$

when the channel cross section is semicircular shaped. The Nusselt number is usually expressed as a function of the Reynolds number Re and the Prandtl number Prthrough correlations. The correlations highly depend on the shape of the fluid flow area. In this study, the straight channels and the zigzag channel designs are considered, and the Nusselt number expression for both designs is respectively stated in Tables 1 and 2. All the correlations stated below are selected for their relevant accuracy and they cover a large range of Reynolds number without overlapping. Thus, all of them are used in the study. Regarding the expression of the Nusselt number in zigzag channels, Fig. 5 shows the geometric parameters.

The Gnielinski correlation gives an expression of the Nusselt number for the turbulent flow regime. It involves the Fanning friction factor f since the friction enhances the heat transfer performance. Similar to the Nusselt number, it depends on the

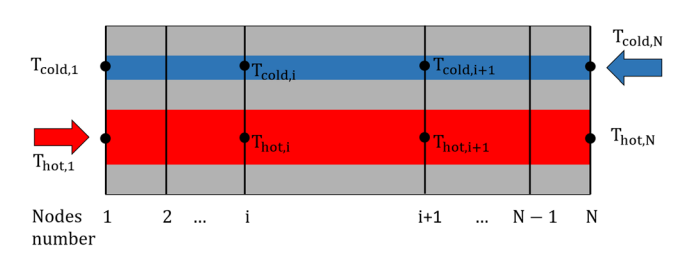


Fig. 4 Discretization of the PCHE into small elements along the flow direction

Table 3 Fanning friction factor correlations in a straight channel [16]

Correlation	Expression
Hesselgreaves	$f = \frac{15.767}{\text{Re}}$
	$Re \leq 2300$
Filonenko	$f = \frac{1}{4(0.79\ln(\text{Re}) - 1.64)^2}$ $2300 \le \text{Re}$

Reynolds number and the shape of the channel. Its expressions for straight and zigzag channels are summarized in Tables 3 and 4.

The governing equations between the $4N_{\Delta x} - 2$ nodal temperatures and the mass flow rates are for $i \in 1, ..., N_{\Delta x}$

$$\dot{m}[H_{i} - H_{i+1}] = A_{\Delta x} h \left(\frac{T_{i} + T_{i+1}}{2}\right) \left|\frac{T_{i} + T_{i+1}}{2} - T_{w,i}\right| \tag{4}$$

$$T_{\text{w,hot,i}} - T_{\text{w,cold,i}} = \dot{m}[H_{\text{i}} - H_{\text{i+1}}] \frac{R^*(\mathbf{\Omega})}{\lambda_{\text{s}} \Delta_{\text{x}}}$$
 (5)

where H_i is the fluid enthalpy at the i-th node, Δ_x is the length of an element and R^* the dimensionless radial conduction resistance whose expression is provided by Kim et al. [18] and depends on the geometry of the elementary heat transfer unit $\Omega = (d_{hot}, d_{cold,...})$. These equations are available for both cold and hot fluids. The system of equations is closed with the boundary conditions. It was found that due to the nonlinearity of Eqs. (4) and (5), the system should be overconstrained to admit a unique solution.

The equations mentioned above are solved in *Python* with the trust region reflective method incorporated in SciPy. The thermal properties of CO₂ and sCO₂ are evaluated with the CoolProp wrapper 6.5.0 [19]. Even though properties are supposed to be independent of the pressure, the pressure profile is not uniform and the pressure drop between the inlet and the outlet quantify the PCHE

Table 4 Fanning friction factor number correlations in a zigzag channel [17]

Correlation	Expression
Yoon	$f = \frac{15.78}{\text{Re}} + \frac{6.7268}{1000} e^{6.6705 \cdot \alpha} \left(\frac{l_r}{d_h}\right)^{-2.3833 \cdot \alpha + 0.26648} + \frac{4.3551 \cdot \alpha - 1.0814}{100}$ $50 \le \text{Re}$ $5 \text{ deg } \le \alpha \le 45 \text{ deg}$ $4.09 \le \frac{l_r}{d_h} \le 32.73$

flow performance. In this study, the pressure drop between two nodes is calculated as

$$\Delta P = \frac{2 \cdot \Delta_{\rm x} \cdot \dot{m}^2 \cdot f}{d_{\rm h} \cdot \rho \cdot A_{\rm cs}^2} \tag{6}$$

where \dot{m} is the mass flow rate in a channel, ρ is the fluid density, and $A_{\rm cs}$ is the fluid cross section area.

An ideal heat exchanger is supposed to transfer a decent amount of energy while keeping the pressure drop at its minimum. These two phenomena are usually quantified through the thermal effectiveness and the Fanning factor. Then, the objective function should minimize the ratio of the two chosen quantities. For instance, Xu et al. [20] used a linear combination of thermal effectiveness reciprocal with the Fanning factor. However, Kwon et al. [21] drew attention to the fact that the objective function equally weights the heat transfer and the pressure drop. More generally, minimizing such combination can lead the PCHE to be economically unsustainable. As a substitute, Kwon et al. performed a PCHE optimization with the total cost depreciated for an operation period of over 20 years as an objective function. The total cost includes production costs and operation costs. The production costs are a direct function of the required material quantity and the etching process, while the operation costs are linked to the pumping power W_{pump} calculated as

$$W_{\text{pump}} = \Delta P \frac{\dot{m}_{\text{total}}}{\rho} \tag{7}$$

Since the total volume is fixed in this study, the quantity of material is constant through the study. Thus, optimizing the PCHE only consists in reducing the required pumping power to maintain the pressure in the pipes for a fixed global geometry and for a constant heat power. Therefore, the objective function is

$$F_{\text{obj}}(\Omega, T_{\text{cold,inlet}}) = W_{\text{pump,hot}} + W_{\text{pump,cold}}.$$
 (8)

Finally, the optimization of the PCHE consists of reducing the objective function $F_{\rm obj}$. To that end, an algorithm of minimization is used. It was found, that most of gradient-based methods failed to converge as the continuity of the derivatives of $F_{\rm obj}$ may not be guaranteed. Thus, the Nelder–Mead method, which is a simplex-based method, was chosen to find the optimized geometry. A flowchart of the optimization process is shown in Fig. 6.

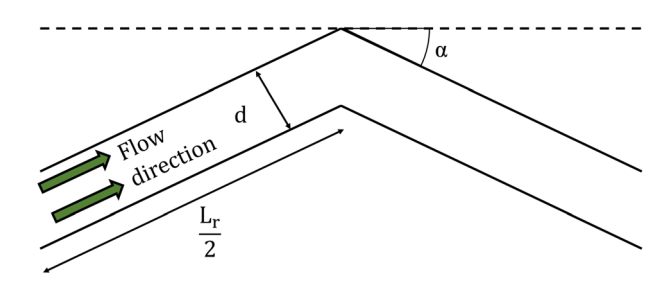


Fig. 5 Geometric parameters for the zigzag channel correlations

2.2 Computational Fluid Dynamic. In order to ensure the validity of the presented model, CFD simulations are performed with the software ANSYS CFX. As the flow is in steady-state, the RANS equations are used, given as

$$\frac{\partial}{\partial \mathbf{x_i}}(\rho \overline{\mathbf{u_j}}) = 0 \tag{9}$$

$$\frac{\partial}{\partial x_{j}}(\rho \overline{u_{i}u_{j}}) = -\frac{\partial \overline{p}}{\partial x_{i}} + \frac{\partial}{\partial x_{j}} \left((\mu + \mu_{t}) \left(\frac{\partial \overline{u_{i}}}{\partial x_{j}} + \frac{\partial \overline{u_{j}}}{\partial x_{i}} \right) \right) \tag{10}$$

$$\frac{\partial}{\partial x_{j}} \left(\rho \overline{u_{j}} \overline{H_{tot}} \right) = \frac{\partial}{\partial x_{j}} \left(\lambda_{f} \frac{\partial \overline{T}}{\partial x_{j}} + \frac{\mu_{t}}{P r_{t}} \frac{\partial \overline{H_{tot}}}{\partial x_{j}} \right) \tag{11}$$

The turbulent Prandtl number Pr_t is often supposed constant, equal to 0.85 for traditional fluid such as air or water, and Liu et al. [22] showed that this hypothesis is still valid for sCO₂. Numerous studies were conducted to simulate PCHEs with CFD. The k- ϵ model is the most common one used in general CFD problems

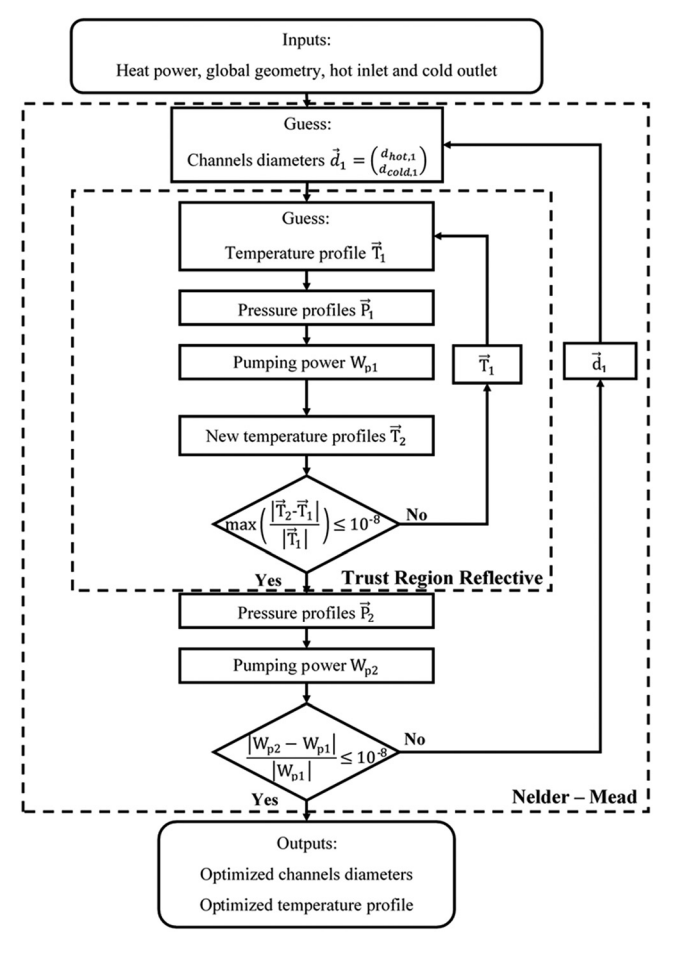


Fig. 6 Flow chart of the optimization process

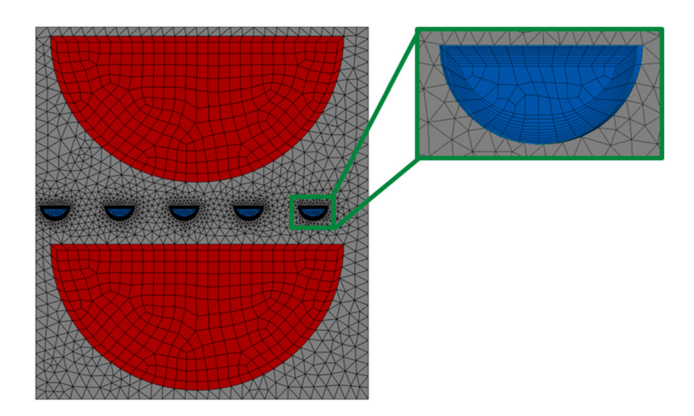


Fig. 7 Cross-section view of the meshing used for the CFD simulation

thanks to its simplicity and relative efficiency [21]. However, Van Abel et al. [23] showed that the k- ε model can underestimate the flow resistance by 30%. For the case of PCHE, most of studies including Zhang et al. [24] recommend using the Shear Stress Transport (SST) k- ε for its good accuracy as long as the dimensionless value y^+ value is approximatively equal to 1. In the present study, the value y^+ ranges from 0.73 to 3.07. Cold channels and hot channels were meshed with hexahedrons and prisms, whilst the solid part was distinctly meshed with either hexahedrons and prisms or tetrahedrons.

Figure 7 shows a cross section view of the considered mesh. One can see how the boundary layer is meshed in the semicircular channel. The simulation is considered mesh-independent when the reduction of the mesh element size has no more significant impact on the outcome, such as the pressure drop and the outlet temperature. The solving scheme is selected on "high resolution" in CFX-Pre.

For the data processing after simulation, the variables are calculated by averaging over surfaces that intersect the channels in cross section. The temperature is obtained by calculating the bulk temperature, defined as

$$T_{b} = \frac{\int_{S} \rho CpuTds}{\int_{S} \rho Cp}$$
 (12)

3 Results and Discussion

3.1 Optimization With the One-Dimensional Model. The optimization process was performed according to the following inputs (Table 5), where a pinch point temperature of 10 K is set. The values are considered constant throughout the study.

As a preliminary result, it was found that the pump power needed to compensate the pressure drop increases with the inlet temperature of the cold fluid (Fig. 8). In fact, the mass flow rate becomes less when the temperature difference between the inlet and the outlet increases, regardless of the geometry. As a result, the velocity in the channel decreases. Since, this temperature is mostly linked to the power cycle design, it is set to 400 °C for the rest of the study. On the other hand, the hot outlet temperature is set to be variable in order to minimize the objective function.

Table 5 Values used as an input for the optimization process

Input	$T_{ m hot,in}$	$T_{\rm cold,out}$	$P_{ m hot,in}$	$P_{\rm cold,in}$	$Q_{ ext{total}}$
Unit	°C	°C	bar	bar	MW
Value	600	590	1	210	1

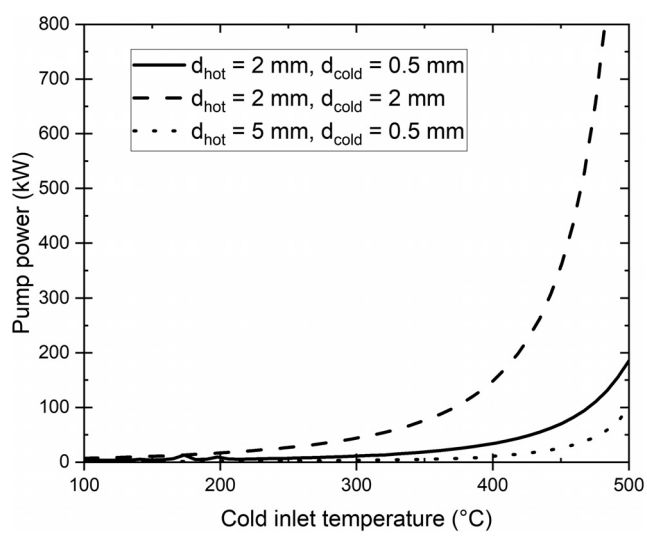


Fig. 8 Evolution of the required pump power against the cold inlet temperature for different geometries in case of straight channels

Table 6 Main characteristics of the optimized geometry for the single banking configuration

Output	$T_{ m hot,out}$	$d_{ m hot}$	d_{cold}	$W_{ m p,hot}$	$W_{ m p,cold}$
Unit	°C	mm	mm	W	W
Value	458	4.72	0.56	8646.4	1580.9

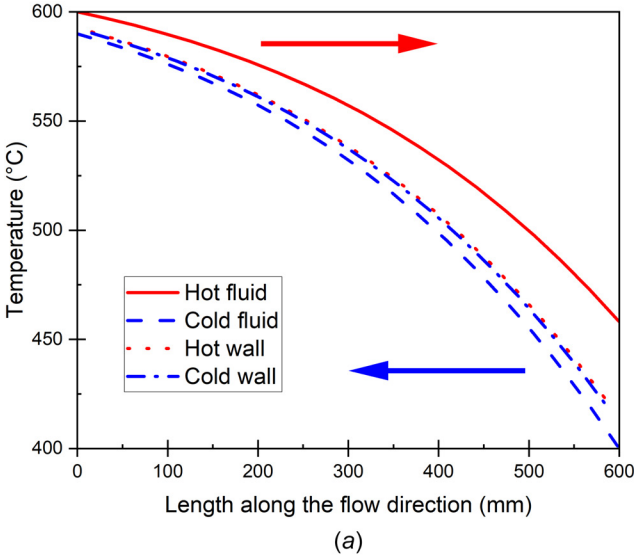
As a first throw, the single banking configuration with one hot channel and one cold channel is studied. Table 6 summarizes the main outputs of the optimization. Whilst the pressure drops in the hot and cold channels are, namely, 0.0104 bar and 0.46 bar, resulting in relative pressure drops of 1% and 0.2% of the absolute pressure, the pump power is relatively high. In fact, 10.2 kW of pumping power are required to compensate for the losses. 84.5% of the pumping power occurs on the hot fluid, due to the low density of the atmospheric-pressured CO₂ (Eq. (6)). Regarding the thermal performance of both fluids, the Reynolds number in the hot and cold channels are, namely, 512.5 and 3941.1. Thus, the hot fluid is in laminar regime and the associated Nusselt number is constant. Meanwhile, the cold fluid is in turbulent regime, resulting in high heat transfer coefficient, despite of the high pressure drop.

The associated temperature and pressure profiles are shown in Fig. 9(a). One can see that the hot and cold wall temperatures are nearly equal. That can be explained by a rough estimation of the associated thermal resistance. According to the correlation from Kim et al. [18], the conduction resistance per unit length is evaluated as 0.0632 (m K)/W, whilst the hot and cold convection resistances are esteemed at 0.727 (m K)/W and 0.223 (m K)/W, respectively. Thus, the conduction resistance can be neglected and it is now assumed that the solid temperature is uniform at any given abscissa, hence

$$T_{\text{wall,hot}} \approx T_{\text{wall,cold}}$$
 (13)

In Fig. 9(b), the pressure drop profiles are linear with a slight curvature, attributed to variations in the thermophysical properties of the fluids. However, the overall trends remain linear.

In addition, the difference between the hot and cold channel diameters is considerable. The hot diameter must be large enough to reduce the fluid velocity as well as the pressure drop. Furthermore, the diameter of both hot and cold channels must be small enough to maintain a high number of hot channels, which results in reducing the velocity in the hot channels, as the mass flow rate is divided among more channels.



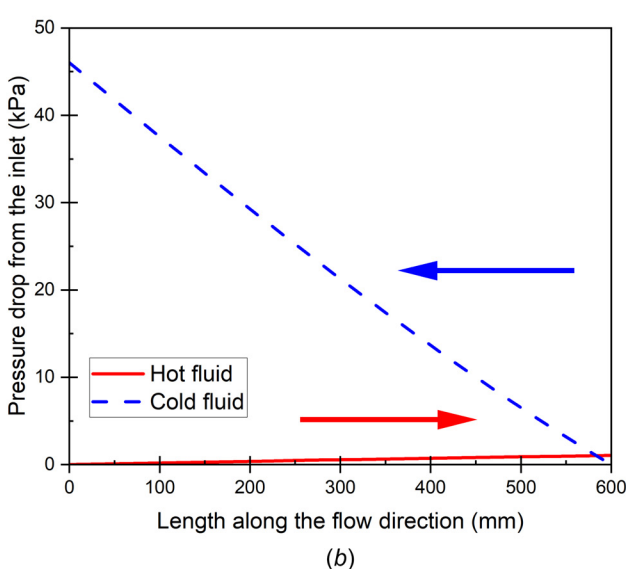


Fig. 9 (a) Evolution of the fluid and wall temperature and (b) pressure drop along the PCHE

This tremendous difference in the diameters shows how ineffective the single banking configuration with one hot channel and one cold channel is. Hence, two other configurations are investigated in this study: the hot channels are kept straight, however double-banked, while the cold channels are either straight or in zigzag. Furthermore, in the light of the diameter difference, more cold channels are fit into an elementary heat transfer unit.

As shown in Table 7, the case B reduces the required pump power by 26% for the hot fluid and 77.9% for the cold fluid from the case A. Since the surface area of the hot channel is doubled and the Nusselt number remains the same, the heat transfer performance improves. Therefore, the temperature difference between the inlet and the outlet increases and the mass flow rate reduces. On the other hand, the channel mass flow rate of the cold fluid is smaller by a factor of 3, and the pressure drop decreases as well. Regarding case C, the heat transfer performance of the cold fluid improves, but the pressure drop is larger due to the zigzag-shape of the channels. Figure 10 shows the values of the local heat transfer coefficient in each case. The hot-side coefficient is low, which is a consequence of a low Reynolds number, and equal to 82 W/(m2K) for each case. However, the cold-side coefficient drastically changes from a case to another, but remains superior to the hot side heat transfer coefficient. In case A and B, the cold fluid flows in a straight channel

Table 7 Overview of the geometry and the performance of the PCHE after optimization for different configurations and designs

Case	Case A	Case B	Case C
Banking configuration	Single	Double	Double
Ratio hot channel/ cold channel	1:1	2:3	2:3
Cold channels design	Straight	Straight	Zigzag
$d_{\rm hot}$ (mm)	4.72	4.8	5.03
$d_{\rm cold}$ (mm)	0.56	0.50	0.51
α (deg)	_	_	17.65
l_r (mm)	_	_	4.0
$W_{\rm p,hot}$ (W)	8646.4	6340.8	4856.6
$W_{\rm p,cold}$ (W)	1580.9	349.0	357.3

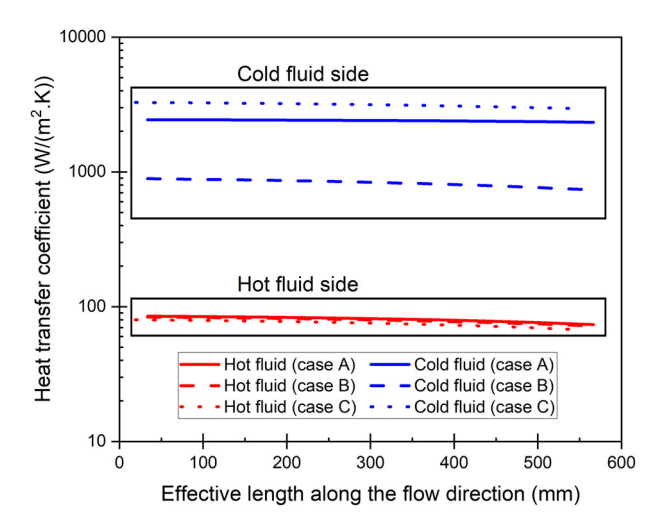


Fig. 10 Local heat transfer coefficient along the PCHE

and in several channels for the case B specifically. That reduces the Reynolds number and thus, the heat transfer coefficient to $2426\,\mathrm{W/m^2\,K}$) and $837\,\mathrm{W/m^2\,K}$). Nonetheless, for an identical mass flow rate, the heat transfer coefficient is increased to $3162\,\mathrm{W/m^2\,K}$) in a zigzag channel.

According to Fig. 11, the total pump power generally reduces when the pressure in the hot fluid increases, mainly due to the rise of CO_2 density at low pressure. For the cases B and C the pump power is lower than for the case A, especially at low pressure. Nonetheless, all three cases, including A, show a convergence of the power at around 200 W, when the hot pressure at the inlet reaches 8 bar. The only

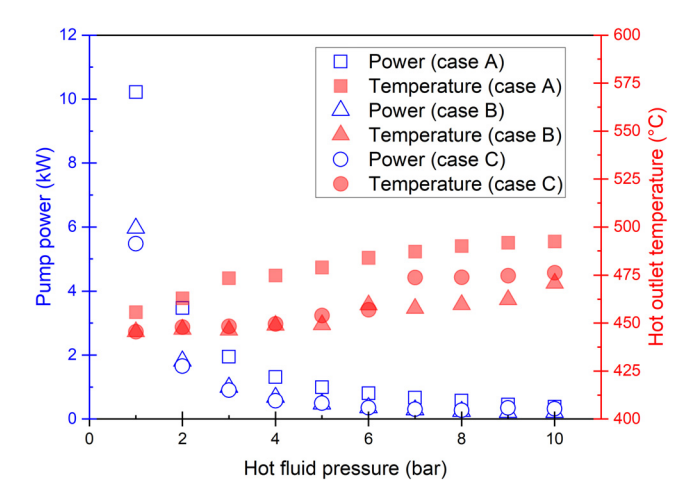


Fig. 11 Total pump power and hot outlet temperature against the hot fluid pressure for the different cases

Table 8 Comparison Between The 1D model and CFD simulation for the case A

	1D	CFD	Relative deviation
$T_{\text{hot,out}}$ (°C)	457.8	455.4	-0.53%
$T_{\text{cold,out}}$ (°C)	590.0	593.3	0.55%
$\Delta P_{\rm hot}$ (kPa)	1.040	1.070	2.88%
$\Delta P_{\rm cold}$ (kPa)	52.00	51.44	-1.08%

Table 9 Comparison between the 1D model and CFD simulation for the Case B

	Channel number	1D	CFD	Relative deviation
$T_{\text{hot,out}}$ (°C)	1	449.6	446.9	-0.60%
not,out ()	2	449.6	447.1	-0.56%
$T_{\text{cold.out}}$ (°C)	1	590	593.6	0.61%
	2	590	593.5	0.59%
	3	590	593.5	0.59%
ΔP_{hot} (kPa)	1	0.8160	0.7995	-2.02%
	2	0.8160	0.7990	-2.08%
$\Delta P_{\rm cold}$ (kPa)	1	10.15	10.13	-0.20%
	2	10.15	10.45	2.96%
	3	10.15	11.01	7.81%

Table 10 Comparison between the 1D model and CFD simulation for the case C

	Channel number	1D	CFD	Relative deviation
$T_{\text{hot,out}}$ (°C)	1	593.4	591.8	-0.27%
	2	593.4	591.7	-0.29
$T_{\text{cold.out}}$ (°C)	1	590.0	590.7	0.12%
	2	590.0	590.8	0.14%
	3	590.0	590.9	0.15%
$\Delta P_{\rm hot}$ (Pa)	1	55.16	53.69	-2.66%
100 ()	2	55.16	53.69	-2.66%
$\Delta P_{\rm cold}$ (Pa)	1	3109	3172	2.03%
,	2	3109	3202	2.99%
	3	3109	3220	3.57%

difference lies in the hot fluid mass flow rate, which tends to be lower when the cases B and C are considered. Therefore, at higher pressure, the choice of the PCHE configurations strongly depends on the requirements for the TES system.

3.2 Comparison With Computational Fluid Dynamics. The three cases mentioned in Table 7 are simulated by CFD and the same boundary conditions were applied. However, the numbers of elements to accurately mesh the case C were too large. Therefore, a shorter version of the heat transfer unit, which includes 12 bends, was simulated by CFD. Thus, the total length of the PCHE in the case C drops from 600 mm to 42.6 mm. The results for the cases A, B and C are, namely, displayed in Tables 8–10, where the pressure differences and the outlet temperatures are compared.

The results from the CFD simulations show that the outlet temperatures are correctly estimated by the model with a margin error inferior to 1% for all three cases. However for the case B, the pressure drop deviation in the straight cold channels ranges from -0.20% to 7.81%, whilst it is 2.88% in case A. The deviation of 7.81% is singular, given that pressure drop is expected to be uniform across all channels. In the zigzag channels, the maximum pressure drop deviation is 3.57%. Since the simulated PCHE is 20 times shorter, there is a potential deviation if the entire channel length is considered. In term of metric pressure drops, zigzag channels exhibit a performance of $72.0\,\mathrm{kPa/m}$, whereas it is $1.26\,\mathrm{kPa/m}$ for straight channels. Figure 12 shows the temperature distribution within the

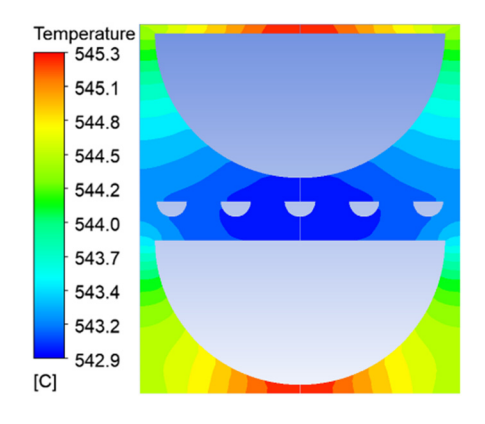


Fig. 12 Temperature distribution in the solid core at the midsection of the PCHE (case B)

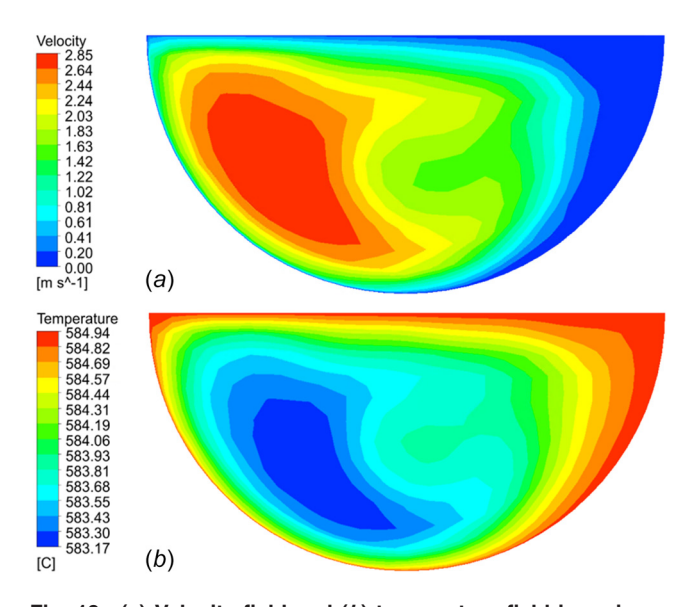


Fig. 13 (a) Velocity field and (b) temperature field in a zigzag channel

solid core in case B. Although the cold channels receive different amounts of power, the difference between the highest and lowest value of temperature is inferior to 4 K. The heat misdistribution does not have a significant impact on the outlet bulk temperatures as depicted by Tables 9 and 10.

Figure 13 shows the velocity and temperature fields in one cold channel, specifically at a bending angle situated 26.7 mm away from the cold outlet in case C. The absolute velocity ranges from 0 to 2.85 m/s, exhibiting asymmetry in its profile due to momentum of the fluid. The associated temperature field follows the shape of the velocity field, fluctuating from 583.17 °C to 584.94 °C. On the other hand, in case B, the temperature field in the cold channel at the equivalent location spans from 582.09 °C to 584.11 °C (Fig. 14), which presents a lower temperature range. In addition, the temperature range is wider with a difference of 2.02 °C between the maximal and the minimal values. This is only 1.77 °C in the zigzag channel as the design enhances the flow mixing, and thus, the heat transfer performance, despite pressure loss.

Thus, the 1D model is able to predict the temperature profile and the pressure drop with a decent accuracy. Different designs, straight and zigzag channels in this study, are mixed and further designs like airfoils and s-shaped fins can be included. However, the model strongly relies on correlations for the Nusselt number and the Fanning factor. It implies that using the correlations outside their range of application may induce significant errors, especially in term of geometrical parameters and Reynolds number. Moreover, some

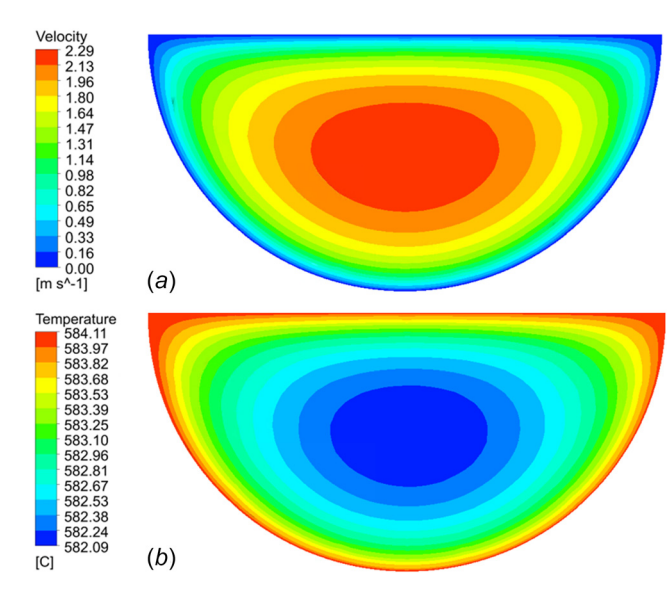


Fig. 14 (a) Velocity field and (b) temperature field in a straight channel

designs lack of correlations that consider the geometry as well, such as the airfoil fins at low Reynolds number.

4 Conclusion

In the present study, the design of a PCHE has been made via a 1D model. The model is able to predict the heat transfer performance and the pressure drop of the PCHE for straight and zigzag channels and a combination of both. Three PCHEs, for which the injected power, the overall geometry and the pinch point temperature were identical, have been optimized by a 1D model. The main results are:

- The pump power required to compensate the pressure drop in the PCHE decreases with increasing hot fluid pressure until 200 W approximately.
- (2) The case A has a worse performance than the cases B and C. For the case B and C the heat transfer surface area increases for a double banking design of the hot channel. However, the difference of the performance between these two cases is negligible.

In addition, CFD simulations have been performed to ensure the validity of the model. It was shown, that the outlet temperatures are accurately estimated within an error of 1%. However, the error due to the pressure drop estimation lies within 7.81%. Despite this deviation, the fluid densities have a relevant impact on the pump power for the hot fluid.

Therefore, the design of a PCHE applying a supercritical working fluid and a gas at atmospheric pressure is subject to significant power losses. Hence, it is essential to study thoroughly the optimization of such heat exchanger in future investigations.

Acknowledgment

This research is part of the project: Novel CO₂-based Electrothermal Energy and Geological Storage system—CEEGS by the HORIZON Action Grant Budget under the Grant No. 101084376. Responsibility of the content of this publication lies with the authors.

Nomenclature

 $A_{\rm cs} = {\rm channel\ cross\ section\ area\ (m^2)}$

 $A_{\Delta x}$ = area of convection surface of an element (m²)

d = semi-circular channel diameter (m)

 $d_{\rm h} = {\rm hydraulic\ diameter\ (m)}$

 $F_{\text{obj}} = \text{objective function to minimize (W)}$

f = fanning friction factor

 H_i = enthalpy at the *i*th node (J/kg)

 $H_{\text{total}} = \text{total height of the PCHE (m)}$

 $h = \text{local heat transfer coefficient } (W/(m^2 K))$

 $L_{\text{total}} = \text{total length of the PCHE (m)}$

 $l_{\rm r} = {\rm subchannel\ length\ (m)}$

 $\dot{m} = \text{mass flow rate in a channel (kg/s)}$

 $\dot{m}_{total} = total \text{ mass flow rate (kg/s)}$

Nu = Nusselt number

 $N_{\Delta x}$ = number of nodes

Pr = Prandlt number

 $Pr_t = turbulent Prandtl number$

 ΔP = pressure difference in a channel (Pa)

 $Q_{\Delta x}$ = power transferred in an element (W)

 R^* = dimensionless conduction resistance (K/W)

Re = Reynolds number

 $T_{\rm b} = {\rm fluid\ bulk\ temperature\ (^{\circ}C)}$

 $T_i/T_{w,i} = \text{fluid/wall temperature at the } i\text{th node } (^{\circ}\text{C})$

 ΔT = temperature difference between the fluid and the wall (K)

 $\overline{u_i} = RANS$ velocity component in the j-direction (m/s)

 $W_{\text{pump}} = \text{pump power related to the pressure drop (W)}$

 $W_{\text{total}} = \text{total width of the PCHE (m)}$

 α = bend angle in zigzag channels (deg)

 $\Delta_{\rm x} = {\rm length~of~an~element~(m)}$

 λ_f/λ_s = fluid/solid thermal conductivity (W/(m K))

 $\mu = \text{dynamic viscosity (Pa} \cdot \text{s)}$

 μ_t = turbulent dynamic viscosity (Pa · s)

 $\rho = \text{fluid density (kg/m}^3)$

 Ω = set of geometric parameters

References

- Agalit, H., Zari, N., and Maaroufi, M., "2020, "Suitability of Industrial Wastes for Application as High Temperature Thermal Energy Storage (TES) Materials in Solar Tower Power Plants – A Comprehensive Review," Solar Energy, 208, pp. 1151–1165.
- [2] Agalit, H., Zari, N., Maalmi, M., and Maaroufi, M., 2015, "Numerical Investigations of High Temperature Packed Bed TES Systems Used in Hybrid Solar Tower Power Plants," Sol. Energy, 122, pp. 603–616.
- [3] Dostal, V., Hejzlar, P., and Driscoll, M. J., 2006, "The Supercritical Carbon Dioxide Power Cycle: Comparison to Other Advanced Power Cycles," Nucl. Technol., 154(3), pp. 283–301.
- [4] Dostal, V., Driscoll, M. J., Hejzlar, P., and Todreas, N. E., 2002, "A Supercritical CO₂ Gas Turbine Power Cycle for Next-Generation Nuclear Reactors," ASME Paper No. ICONE10-22192.
- [5] Liu, Y., Wang, Y., and Huang, D., 2019, "Supercritical CO₂ Brayton Cycle: A State-of-the-Art Review," Energy, 189, p. 115900.
- [6] Yang, J., Yang, Z., and Duan, Y., May 2021, "Load Matching and Techno-Economic Analysis of CSP Plant With S-CO₂ Brayton Cycle in CSP-PV-Wind Hybrid System," Energy, 223, p. 120016.
- [7] Marchionni, M., Bianchi, G., Tsamos, K. M., and Tassou, S. A., 2017, "Techno-Economic Comparison of Different Cycle Architectures for High Temperature Waste Heat to Power Conversion Systems Using CO₂ in Supercritical Phase," Energy Procedia, 123, pp. 305–312.
- [8] Marchionni, M., Bianchi, G., and Tassou, S. A., 2020, "Review of Supercritical Carbon Dioxide (sCO₂) Technologies for High-Grade Waste Heat to Power Conversion," SN Appl. Sci., 2(4), p. 611.
- [9] Kim, H., Kim, H., Lee, S., and Kim, J., 2018, "A Study on Heat Transfer Characteristics of Quinary Molten Salt Mixture," Int. J. Heat Mass Transfer, 127, pp. 465–472.
- [10] Ma, Y., Xie, G., and Hooman, K., "2022, "Review of Printed Circuit Heat Exchangers and Its Applications in Solar Thermal Energy," Renewable Sustainable Energy Rev., 155, p. 111933.
- [11] Shi, H. Y., Li, M. J., Wang, W. Q., Qiu, Y., and Tao, W. Q., 2020, "Heat Transfer and Friction of Molten Salt and Supercritical CO2 Flowing in an Airfoil Channel of a Printed Circuit Heat Exchanger," Int J. Heat Mass Transfer, 150, p. 119006.
- [12] Zhu, Q., Tan, X., Barari, B., Caccia, M., Strayer, A. R., Pishahang, M., Sandhage, K. H., and Henry, A., 2021, "Design of a 2MW ZrC/W-Based Molten-Salt-to-sCO₂ PCHE for Concentrated Solar Power," Appl Energy, 300, p. 117313.
- [13] Marchionni, M., Chai, L., Bianchi, G., and Tassou, S. A., 2019, "Numerical Modelling and Performance Maps of a Printed Circuit Heat Exchanger for Use as Recuperator in Supercritical CO₂ Power Cycles," Energy Procedia, 161, pp. 472–479.
- [14] Lao, J., Fu, Q., Wang, W., Ding, J., and Lu, J., 2021, "Heat Transfer Characteristics of Printed Circuit Heat Exchanger With Supercritical Carbon Dioxide and Molten Salt," J. Therm. Sci., 30(3), pp. 880–891.
- [15] Jiang, Y., Liese, E., Zitney, S. E., and Bhattacharyya, D., 2018, "Design and Dynamic Modeling of Printed Circuit Heat Exchangers for Supercritical Carbon Dioxide Brayton Power Cycles," Appl. Energy, 231, pp. 1019–1032.

- [16] Mylavarapu, S. K., Sun, X., Glosup, R. E., Christensen, R. N., and Patterson, M. W., 2014, "Thermal Hydraulic Performance Testing of Printed Circuit Heat Exchangers in a High-Temperature Helium Test Facility," Appl. Therm. Eng., 65(1–2), pp. 605–614.
- [17] Yoon, S.-J., O'Brien, J., Chen, M., Sabharwall, P., and Sun, X., 2017, "Development and Validation of Nusselt Number and Friction Factor Correlations for Laminar Flow in Semi-Circular Zigzag Channel of Printed Circuit Heat Exchanger," Appl. Therm. Eng., 123, pp. 1327–1344.
- [18] Kim, W., Baik, Y. J., Jeon, S., Jeon, D., and Byon, C., 2017, "A Mathematical Correlation for Predicting the Thermal Performance of Cross, Parallel, and Counterflow PCHEs," Int. J. Heat Mass Transfer, 106, pp. 1294–1302.
- [19] Bell, I. H., Wronski, J., Quoilin, S., and Lemort, V., 2014, "Pure and Pseudo-Pure Fluid Thermophysical Property Evaluation and the Open-Source Thermophysical Property Library Coolprop," Ind. Eng. Chem. Res., 53(6), pp. 2498–2508.
- [20] Xu, H., Duan, C., Ding, H., Li, W., Zhang, Y., Hong, G., and Gong, H., 2021, "The Optimization for the Straight-Channel PCHE Size for Supercritical CO₂ Brayton Cycle," Nucl. Eng. Technol., 53(6), pp. 1786–1795.
- Cycle," Nucl. Eng. Technol., 53(6), pp. 1786–1795.

 [21] Kwon, J. G., Kim, T. H., Park, H. S., Cha, J. E., and Kim, M. H., 2016, "Optimization of Airfoil-Type PCHE for the Recuperator of Small Scale Brayton Cycle by Cost-Based Objective Function," Nucl. Eng. Des., 298, pp. 192–200.
- [22] Ping Huang, Y., Feng Wang, J., and Leung, L. K. H., S. hui Liu 2018, "Numerical Investigation of Buoyancy Effect on Heat Transfer to Carbon Dioxide Flow in a Tube at Supercritical Pressures," Int J Heat Mass Transfer, 117, pp. 595–606.
- [23] Kruizenga, A., Li, H., Anderson, M., and Corradini, M., 2012, "Supercritical Carbon Dioxide Heat Transfer in Horizontal Semicircular Channels," ASME J. Heat Mass Transfer-Trans. ASME, 134(8), p.081802.
- [24] Zhang, Y., Peng, M., Xia, G., and Cong, T., 2019, "Numerical Investigation on Local Heat Transfer Characteristics of S-CO₂ in Horizontal Semicircular Microtube," Appl. Therm. Eng., 154, pp. 380–392.